Nonlinear Stability Analysis for Artificial Kidney Multi-compartmental Models

Rammah Abohtyra CV Hollot, *Fellow*, *IEEE*, J Horowitz, Yossi Chait

***Abstract*—This paper addresses a new global stability analysis for a class of nonlinear multi-compartment models. The stability analysis is applied to a specific physiological two-compartment model used in dialysis therapy in end-stage kidney disease patients. Dialysis is a life-sustaining treatment in which an artificial kidney is used to correct acid-base derangement and remove fluid accumulation by ultrafiltration to obtain dry weight (normal weight without extra fluid). Our stability analysis is motivated by the current emphases on improving the assessment of dry weight and strategies for optimal fluid removal in end-stage kidney disease patients. To gain physiological insights into fluid management during the short time (3-5hrs) of the dialysis therapy, we use this model to examine and analyze the solution's boundedness and behavior under ultrafiltration.**

In this paper we developed global stability results for a class of nonlinear multi-compartment models, which applies to our specific model used in dialysis therapy. The boundedness and behavior of the solution of our model during dialysis therapy is illustrated under ultrafiltration. We tested our results using both standard ultrafiltration and patient-specific ultrafiltration profiles.

***Index Terms*—Nonlinear Stability, Artificial kidney, Dialysis therapy, and Ultrafiltration.**

I. Introduction

Patient in end-stage kidney disease are often suffering from multiple acid-base derangements, and fluid shift complications [10], [25]. Dialysis is a life-sustaining treatment that corrects acid-base derangement and removes fluid accumulation to obtain dry weight (normal weight without extra fluid) [17], [24], [29], [21]. During dialysis treatment, an artificial kidney is used to remove excess fluid from the blood (plasma) by ultrafiltration leading to fluid refilling from the interstitial compartment to overcome the fluid shift [27], [26]. An inadequate balance between fluid removal and refill is associated with increased morbidity, and mortality risk [28].

The current emphasis on improving the assessment of dry weight and strategies for fluid removal in dialysis therapy motivated the need for exploring fluid management and equilibrium to provide possible stabilizing procedures that may offer guidelines for optimal fluid removal strategies in end-stage kidney disease patients.

The total body fluid is distributed mainly between two compartments, the extracellular compartment (ECC), which contains fluid outside the cells including interstitial fluid and plasma (about 20% of the body weight), and the intracellular compartment (ICC) which contains fluid inside the cells, (about 40% of the body weight) [13]. The ECC is divided by a capillary membrane into the interstitial compartment and the intravascular compartment. The intravascular compartment contains blood which consists of cells (e.g., red blood cells) and plasma. The plasma is the noncellular part of the blood [9], [15]. Fluid-exchange between the intravascular and interstitial compartments is controlled by the Starling forces, namely, the osmotic and hydrostatic pressure gradients [6], [8]. If the difference between these gradients is negative, there will be a fluid filtration across the capillary membrane into the intravascular compartment. However, if the difference is positive, resulting in a filtration of fluid into the interstitial spaces.

Over the past years, there has been an active research effort to characterize fluid removal from the intravascular compartment by ultrafiltration and vascular refilling from the interstitial spaces during dialysis treatment. Two-compartment models describing the short-term dynamics of vascular refilling and ultrafiltration have been derived in (e.g.,[4], [6], [18], [30], [31]). For example, the model in [6] provides a simplified linear two-compartment model and nonlinear two-compartment model incorporating the lymphatic system. This work addresses the contribution of lymph flow to the fluid movement from interstitial spaces to the intravascular compartment. More recently, in [4], a nonlinear two-compartment model was developed to describe the vascular refilling during dialysis. This model considers (microvascular) fluid shifts between the compartments and lymph flow from the interstitial to the intravascular compartment.

There are many methods for analyzing stability of nonlinear compartmental models [16] and others. Among them is the Lyapunov stability approach. Exploring stability of nonlinear compartment model with Lyapunov method is a challenging task because it often requires searching for Lyapunov candidate by trial-and-error. Stability of a class of nonlinear compartment models, based on the Lyapunov approach, has been investigated in [5], [14], [16]. Since the fluid flow of our model is non-positive, the results of these papers cannot be applied to our model because of the particular class of models under consideration.

A class of nonlinear compartment model, similar to our model, has been discussed in [22], [23]. Sufficient conditions concerning the flows between the compartments are made (positive flow). These results, however, do not seem to be applicable to our model because the conditions are not satisfied, and the Lyapunov functions used are inappropriate for our model. In addition, another class of nonlinear models has been studied in [7]. Although these models have a similar structure to ours, the result of [7] is not applicable here because it pertains only to isolated equilibrium points. The above compartmental models were used with external inputs

described by a specific class of constant non-decreasing input and with sufficient conditions to extend stability results.

Our contribution in this paper is two folds. First, we overcome these limitations, and provide a new Lyapunov function to prove global stability of a general class of nonlinear compartment model whose flow functions are non-positive. These results are applied to our specific two-compartment model used for dialysis therapy in patients with kidney failure. Second, we extend the results to include the effect of the input on the model to investigate the boundedness and behavior of the solution of the nonlinear model under ultrafiltration.

We organize the paper as follows: We begin by introducing the two main fluid compartments. In Section II, a brief description of the fluid-exchange of an artificial kidney two-compartment model is presented. In Section III, global stability analysis is provided including the main results. In Section IV, simulation examples are provided. Finally, in Section V is the conclusions.

II. Artificial Kidney Model description

The two-compartment model represented by Fig. 1 is comprised of the intravascular and interstitial compartments, which are separated by a capillary membrane wall, and lymphatic flow which returns a small amount of fluid from the interstitial compartment into the intravascular compartment [12]. Because the plasma is the extracellular fluid part of the blood contained in the intravascular compartment, in this paper, we consider that the plasma volume is part of the intravascular compartment volume. There is a continuous microvascular fluid filtration/refilling between the intravascular and interstitial compartments via the capillary membrane where K_f refers to filtration/refilling coefficient [L/min.mmHg].

- Input: The ultrafiltration rate (UFR) is the external input to this model (denoted by u with negative sign), which describes the fluid removal from the intravascular compartment (i.e., plasma) during dialysis treatment.
- Output: The hematocrit (Hct) is the measured output, which is the proportion of the total blood volume that consists of red blood cells (RBCs); Hct is usually expressed as a percentage in clinical practices but is expressed here as a fraction.

The mathematical description of this model during dialysis is given by nonlinear differential system:

$$\dot{x}_1 = -Q_1(x_1, x_2) + Q_2(x_2) - u \tag{1a}$$

$$\dot{x}_2 = Q_1(x_1, x_2) - Q_2(x_2) \tag{1b}$$

$$Hct = \frac{V_{rbc}}{V_{rbc} + x_1} \tag{1c}$$

where $x = (x_1, x_2)$ is the state of the model, x_1 and x_2 represent the intravascular and interstitial volume, respectively; and V_{rbc} is the volume of the red blood cells; $Q_1(x)$ denotes the flow of the fluid filtration/refilling between the two-compartments across the capillary membrane, which is governed by the Starling's equation [4]; $Q_2(x_2)$ describes the lymphatic flow, we have

$$Q_1(x_1, x_2) = K_f(\delta_p - \delta_\pi) \tag{2a}$$

$$Q_2(x_2) = g\tanh(hP_i) + l \tag{2b}$$

where δ_p and δ_π represent the hydrostatic and osmotic pressure gradients, respectively. The mathematical descriptions of these functions are given in the Appendix A. g, h, and l are constants listed in Table I. During the fluid exchange between the two compartments, $Q_2(x_2)$ is smaller that $Q_1(x)$ [12].

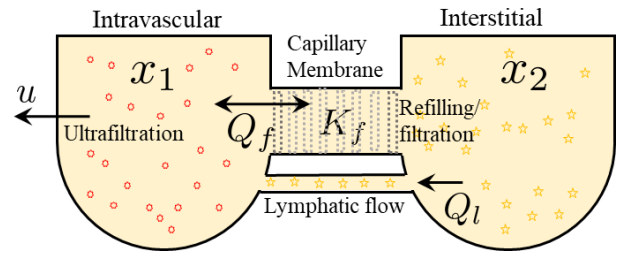

Figure 1. Two-compartment model used for the artificial kidney treatment, contains: interstitial and intravascular compartments separated by a capillary membrane, and includes lymph flow and ultrafiltration.

III. Stability Analysis For General Class of Compartment Models

The class of nonlinear compartment models that we are dealing with in this paper is developed in [5], [22], [23]. In order to derive a general stability result (Theorem 1 below) for this class, we consider n compartments where the dynamics of a certain amount of a material of interest in the ith compartment at time t, denoted by $x_i(t)$, is given by

$$\dot{x}_i(t) = -a_{ii} f_i(x_i(t)) + \sum_{j \neq i} a_{ij} f_j(x_j(t)) + u_i \tag{3}$$

where $a_{ij} \geq 0$, $i, j \in \{1, \ldots, n\}$. The ith compartment receives the material through the input at rate u and from some other neighboring compartments (e.g., jth) at rate $a_{ij} f_j(x_j(t))$ where the nonlinear function $f_j(x_j)$ depends on the concentration of the jth compartment x_j.

Note that all the results of stability in these studied [5], [22], [23] were based on the assumption that $f_{ij}(x_j) \geq 0$, for $x_j \geq 0$, $1 \leq i, j \leq n$, $i \neq j$ and $f_{ij}(0) = 0$. However, these results do not imply to the model in (1) because $Q_1(x) \leq 0$ and the nonlinear functions $Q_1(x)$ and $Q_2(x_2)$ defined in (2a) and (2b), respectively, are not continuous in the entire domain of $x \in \mathbb{R}^2$. This readily can be seen from (15), in words at the origin ($x \equiv 0$). The dynamics in (3) with n compartments has a more compact form, which can be written as

$$\dot{x} = A_n f(x) + Bu, \quad x_0 \neq 0 \tag{4}$$

where $f(x) = [f_1(x_1), \ldots, f_n(x_n)]^T$, B is an I_n identity matrix, and the matrix $A_n \in \mathbb{R}^{n \times n}$ is a symmetric matrix (i.e., $a_{ij} = a_{ji}$) defined by

$$A_n = \begin{bmatrix} -a_{11} & a_{12} & \cdots & a_{1n} \\ a_{21} & -a_{22} & \cdots & a_{2n} \\ \vdots & \ddots & \ddots & \vdots \\ a_{n1} & \cdots & a_{n,n-1} & -a_{nn} \end{bmatrix}.$$

Note that the nonlinear function of the flow $Q_1(x_1, x_2)$ (2a) depends on both states x_1 and x_2, whereas, in the general form (3), the flow of the compartment i, (i.e., $f_i(x_i)$), depends only

on the associated state x_i. We illustrated the rearrangement of Q_1 in the form of (3) in the next section.

A. Compact Form and Equilibrium Set

It is possible to rearrange the model (1) in the compact form of (4) by rearranging the equation of $Q_1(x)$ with $Q_2(x_2)$. This rearrangement is explicitly derived in the Appendix in B, (16). The compact form of the model in (16) is:

$$\dot{x} = A_2 g(x) - u, \quad x_0 \neq 0 \tag{5}$$

where $g(x) = [\ g_1(x_1) \quad g_2(x_2)\ ]^T$ and A_2 is symmetric, negative semi-definite given by

$$A_2 = \begin{bmatrix} -1 & 1 \\ 1 & -1 \end{bmatrix}.$$

The mathematical description of $g_1(x_1)$ and $g_2(x_2)$ are detailed in Appendix B, (16). Because both of these functions are not continuous in the entire domain of $x \in \mathbb{R}^2$, we specify a restrictive domain as follows by this subset:

$$B := \{x \in \mathbb{R}^2 \mid 5 \geq x_1 \geq 1 \text{ and } 28.4 \geq x_2 \geq 5\} \tag{6}$$

This closed subset is started at (1, 5) liters and closed at (5, 28.4) liters, which is illustrated by Fig. 2. A brief description is provided in the Appendix A about how we specified this subset.

To obtain an equilibrium point (x_{eq}), we assume that there is no UFR ($u \equiv 0$), then we solve for $g_1(x_{1eq}) = g_2(x_{2eq})$ where this equality occurs at equilibrium: $0 = A_2 g(x_{eq})$. Due to high nonlinearity in these functions: $g_1(x_1)$ and $g_2(x_2)$, we could not derive an explicit expression, analytically, for the equilibrium point, x_{eq}, however, we compute instead an equilibrium set E, numerically, as shown in Fig. 2, by defining x_1 and x_2 which satisfy the following relation: $g_1(x_1) = g_2(x_2)$.

We define the equilibrium set for the model in (5) as follows:

Definition 1. Consider model (5) with $u \equiv 0$, the equilibrium set of (5) is define by

$$E := \{x \in B \mid A_2 g(x) = 0\}$$

in which $g_1(x_1) = g_2(x_2)$.

By defining the net flow as: $G(x) = -g_1(x_1) + g_2(x_2)$, we can introduce two subsets above and below E, described by $E^+ := \{x \in B \mid G(x) > 0\}$ and $E^- := \{x \in B \mid G(x) < 0\}$, as shown in Fig. 2.

IV. Results

Our stability results in this section is discussed as follows:

1) Deriving new global stability results for the general class of nonlinear model (4) using an appropriate Lyapunov function. This model consists of n compartments and with zero input ($u \equiv 0$), i.e., $\dot{x} = A_n f(x)$, $x_0 \neq 0$. Then we apply this result to our model in (5).
2) Under nonzero input $u \neq 0$ (UFR) and certain physiological conditions, we demonstrate the boundedness of the solution $x(t)$ of (5) during $0 \leq t < \infty$. Specifically, we use qualitative properties of $G(x)$ and under various forms of UFR profiles used in dialysis therapy to ensure that the solution $x(t)$ of (5) is contained in a closed pre-defined set during $t \geq 0$ and then as $t \to \infty$, $x(t)$ approaches the equilibrium set E.

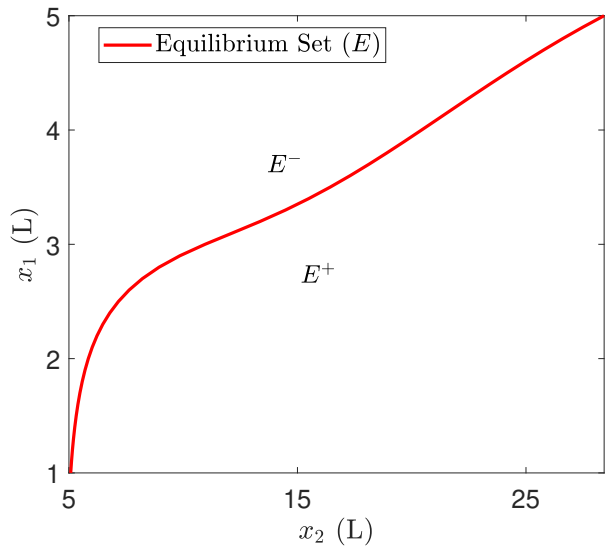

Figure 2. The equilibrium set E of the model (5) for all $x \in B$, including E^+ and E^- subsets. E starts at an equilibrium point (1, 5) and ends at this equilibrium point (5, 28.4).

A. Global Stability Results

The fluid volume in each compartment of our model has a dynamics defined in (5). This dynamics can be determined by a certain slope s. When $u \equiv 0$ in (5), the slope is given very simply as follows:

$$s = \dot{x}_2 / \dot{x}_1 \tag{7}$$

Lemma 1. *When $u_1 \equiv 0$ in (5), the slope $s = -1$ for all $x \in B - E$.*

Proof: We substitute $\dot{x}_1$ and $\dot{x}_2$ from (5) into (7), thus

$$s = \frac{-g_1(x_1) + g_2(x_2)}{g_1(x_1) - g_2(x_2)} = \frac{G(x)}{-G(x)} = -1, \forall x \in B - E$$

■

Note that for all points in E, by definition $\dot{x}_1 = 0$, $\dot{x}_2 = 0$, consequently, the slope is undefined.

We will establish the global stability result of the general compartment model in (4). For this purpose, we invoke LaSalle's Theorem since it is applicable to system having an equilibrium set rather than an isolated equilibrium point [19]. The main results of this paper are demonstrated in Theorem 1 and Theorem 2, by which nonlinear stability of a general class of compartment models (4) and the boundedness of the solution of (5) are explored.

Theorem 1. *Consider (4) with $u \equiv 0$ and let $\Omega \subset \mathbb{R}^n$ be compact and positively invariant with respect to the system in (4). Assume $f(x)$ is differentiable in Ω, and let E be the equilibrium set $E = \{x \in \Omega \mid A_n f(x) = 0\}$, and let $\frac{\partial f_i(x_i)}{\partial x_i} > 0$, $i = 1, \ldots, n$, $\forall x \in \Omega$. If $x_0 \in \Omega$, then $x(t)$ approaches E as $t \to \infty$.*

Proof: Consider the Lyapunov function candidate: $V(x) : \mathbb{R}^n \to \mathbb{R}$ defined by

$$V(x) = -\frac{1}{2} f(x)^T A_n f(x) \tag{8}$$

where this function is continuous, differentiable. Note $f(x)$ and A_n are given in (4). The derivative of $V(x)$ with respect to the time is derived in the Appendix C as

$$\dot{V}(x) = -\sum_{i=1}^{n} \dot{x}_i^2 \frac{\partial f_i(x_i)}{\partial x_i} \tag{9}$$

where $\dot{x}_i$ is defined in (3). This function satisfies the following conditions:

- $\dot{V}(x) \leq 0, \forall x \in \Omega$,
- $\dot{V}(x) = 0, \forall x \in E$.

In fact, E is the largest invariant subset in which $\dot{V}(x) = 0$, this can be shown as follows. Obviously E is a subset of $\{x \in E \mid \dot{V}(x) = 0\}$. Now suppose x is such that $\dot{V}(x) = 0$. Then by (9) $\dot{x}_i = \dot{V}(x) = 0$ for all i, therefore, $x \in E$. It follow by LaSalle's Theorem (Theorem 4.4 in [32]), that $x(t)$ converges to E. ■

In the next subsection, we will invoke Theorem 1 to prove global stability of the fluid volume two-compartment model.

B. Application to Two-compartment Model

We will demonstrate the attractivity of the equilibrium set of the two-compartment model which defined in (5). To invoke Theorem 1, we consider model (4) with $n = 2$. For this model, the $\frac{\partial f_i(x_i)}{\partial x_i} > 0$, $i = 1, 2$, $\forall x \in B$ for the parameters given in Table I. Consider the Lyapunov function:

$$V(x) = -\frac{1}{2} g(x)^T A g(x)$$

where in this case, matrix A is as defined in (5). Then

$$\dot{V}(x) = -\sum_{i=1}^{n=2} \dot{x}_i^2 \frac{\partial g_i(x_i)}{\partial x_i}$$

where $\dot{x}_i$, $i = 1, 2$ are given in (1). We simplify $\dot{V}$ as

$$\begin{aligned}
\dot{V}(x) &= -\dot{x}_1^2 \frac{\partial g_1(x_1)}{\partial x_1} - \dot{x}_2^2 \frac{\partial g_2(x_2)}{\partial x_2} \text{ where } (\dot{x}_2 = -\dot{x}_1) \\
&= -\dot{x}_1^2 \frac{\partial g_1(x_1)}{\partial x_1} - (-\dot{x}_1)^2 \frac{\partial g_2(x_{12})}{\partial x_2} \\
&= -\dot{x}_1^2 \frac{\partial g_1(x_1)}{\partial x_1} - \dot{x}_1^2 \frac{\partial g_2(x_2)}{\partial x_2}, \text{ which yield to} \\
\dot{V}(x) &= -\dot{x}_1^2 \left(\frac{\partial g_1(x_1)}{\partial x_1} + \frac{\partial g_2(x_2)}{\partial x_2} \right) \leq 0, \forall x \in B
\end{aligned}$$

By construction the subset B is a compact set. To show that B is a positively invariant set with respect to model (5), from (Lemma 1) if $x_0 \in B$, then $x(t)$ approaches E as $t \to \infty$ with a particular slope and direction such that $x(t)$ never leave B.

C. Boundedness of Solutions with Nonzero Input

To examine the boundedness of the solution of (5) under nonzero input ($u \neq 0$), we use qualitative properties of $G(x)$ under the effect of UFR profile.

For this purpose, we derive the partial derivatives $G_{x_1} = \frac{\partial G(x)}{\partial x_1}$ and $G_{x_2} = \frac{\partial G(x)}{\partial x_2}$ (see Appendix D) where $G(x)$ is defined previously as $G(x) = -g_1(x_1) + g_2(x_2)$. We also define the target volume to be removed as V_T (L), and $U(t) \equiv \int_0^t u(\tau) d\tau$ (L) is the total amount of fluid volume removed at time t determined by accumulating UFR (u) during $[0, t]$; therefore, the removed fluid volume at the end of a HD session is $U(t_f) \equiv \int_0^{t_f} u(\tau) d\tau$ (L) where t_f is the duration of the dialysis session; $V(t) = x_1(t) + x_2(t)$ (L) is defined as the total fluid volume in the system at time t; $V_0 = x_{10} + x_{20}$ (L) is the initial fluid volume in the system. Theorem 2 demonstrates that the solution $x(t)$ of (5) is bounded and contained in a per-defined closed set: $B_m := \{x : 0 \leq G(x) \leq u_{max}, x_1 \leq x_{10}, x_2 \leq x_{20},$ and $(x_1 + x_2) > V_0 - U(t_f)\}$.

In this set, we use physiological values (from dialysis therapy) for UFR profile, u_{max}, x_{10}, x_{20}, and t_f to examine the boundedness of the solution $x(t)$ for $t \geq 0$ and as $t \to \infty$ (i.e., $t > t_f$), thus $x(t)$ approaches E.

Theorem 2. *Consider (5) with $x_0 \in E$ where $E := \{x \in B : G(x) = 0\}$. Let $E^+ := \{x : G(x) > 0\}$. Suppose G is continuous on the interior of the 1st quadrant and satisfies the following:*

1) $G_{x_1} < 0$, $\forall x \in E \cup E^+$.
2) $G_{x_2} > 0$, $\forall x \in E \cup E^+$.

A) For given: $0 < u_{max} < U_0$, $V_T \leq x_{10}$, $u(t) \geq 0$, and $t_f > 0$, take input $u_1(t)$:

$$u_1(t) = \begin{cases} u_{max}, & 0 < t \leq t_f \\ 0 & t > t_f \end{cases} \tag{10}$$

B) For given: $0 < u_{max} < U_0$, $V_T \leq x_{10}$, $\hat{u}(t) \geq 0$, and $t_f > 0$, take input $u_2(t)$:

$$u_2(t) = \begin{cases} u_{max}, & 0 < t \leq t^* \\ \hat{u}(t) \leq u_{max}, & t^* < t \leq t_f \\ 0 & t > t_f. \end{cases} \tag{11}$$

Let $x(t)$ be a solution to (5) and let B_m be: $B_m := \{x : 0 \leq G(x) \leq u_{max}, x_1 \leq x_{10}, x_2 \leq x_{20},$ and $(x_1 + x_2) > V_0 - U(t_f)\}$. Then $x(t) \in B_m$ for all $0 \leq t \leq t_f$.

The prove of Theorem 2 is provided in the Appendix E.

We will illustrate this result by considering the following numerical examples.

V. Simulation Examples

To test our results of the solution boundedness under a nonzero input, we consider the model in (5) with different UFR profiles applied to the system, including constant UFR profile, step UFR profile, and patient-specific (time-varying) UFR profile developed in our previous work [1], as shown in Fig. 3.

In Theorem 2 we give physiological conditions under which the solution $x(t)$ is contained in this set B_m where $B_m :=$

$\{x : 0 \leq G(x) \leq u_{max}, x_1 \leq x_{10}, x_2 \leq x_{20},$ and $(x_1+x_2) > V_0 - U(t_f)\}$. During $0 \leq t < t_f$, $x(t)$ will be bounded in this region: $0 \leq G(x) \leq u_{max}$ where u_{max}, which describes the maximum UFR rate should be in this range $u_{max} \leq 13$ ml/hr/kg to minimize cardiovascular risk [3]. We chose the duration of the dialysis treatment to be t_f = 4 hrs. The UFR profiles in Fig 3 were given to remove target fluid volume as follows: 4L, 4.5L, and 4L, respectively.

The initial conditions (initial volumes) for these dialysis sessions were determined to satisfy this condition: $V_T \leq x_{10}$ (Theorem 2), which means that the target dialysis volume to be removed by UFR is bigger than or equal to the initial plasma volume x_{10}. This condition allows to begin the dialysis therapy with initial fluid volume $V_0 = x_{10} + x_{20}$ that is a large enough to keep $x(t)$ inside the set B_m during $0 \leq t < t_f$. As we illustrated in Fig. 4 and 6, since $V_T = 4$L, we began at the same initial conditions $(4, 20.4)$L on E, whereas, for the step UFR profile in Fig. 5, the initial conditions were at $(4.5, 24.2)$L because the target volume was $V_T = 4.5$L.

The time-varying UFR profile (Fig. 3, bottom) was designed to use a higher UFR rate (0.027L/min, which is 1.62 L/hr) to remove more fluid in the first one-third of the session when the fluid refilling rate is high, and then the UFR was decreased slightly towards the end of the session when the refilling rate could be low. However, the step UFR profile was increased in the second half of the therapy, which is not recommended in clinical practices because it may provoke the intradialytic hypotension (intradialytic systolic blood pressure (SBP) < 90 mmHg) [2].

We illustrated the boundedness of $x(t)$ under the three UFR profiles as shown in the Phase-plane figures: Fig. 4, 5, and 6. The solution $x(t)$ of (5) was contained in these sets during the entire time frame $0 < t \leq t_f$, respectively:

$$\begin{aligned} B_{m1} :=& \{x : 0 \leq G(x) \leq 0.017 \text{ [L/min]}, x_1 \leq 4\text{L}, \\ & x_2 \leq 20.4\text{L}, \text{ and } (x_1 + x_2) > 20.4\text{L}\} \\ B_{m2} :=& \{x : 0 \leq G(x) \leq 0.023 \text{ [L/min]}, x_1 \leq 4.5\text{L}, \\ & x_2 \leq 24.2\text{L}, \text{ and } (x_1 + x_2) > 24.2\text{L}\} \\ B_{m3} :=& \{x : 0 \leq G(x) \leq 0.027 \text{ [L/min]}, x_1 \leq 4\text{L}, \\ & x_2 \leq 20.4\text{L}, \text{ and } (x_1 + x_2) > 20.6\text{L}\} \end{aligned}$$

To provide physiological insights and a better understanding of fluid removal during the dialysis treatment, we explore the behavior of the solution $x(t)$ inside the set B_m under these UFR profiles. From the solution's trajectory $x(t)$, there was a reduction in the fluid volume in both directions (x_1, x_2) under the constant and step function UFR profiles. This reduction was significantly appeared under the step function UFR profile Fig. 5, due to the step increased in the UFR. On the other hand, the time-varying UFR profile, which removed the same amount of fluid as the constant UFR profile (4L), showed an opposite effect on the trajectory of $x(t)$. The trajectory was considerably increased during the second-third of the session as shown in Fig. 6, due to the decrease in the UFR, to prevent the occurrence of intradialytic hypotension, which likely appears at the end of each session, due to the lack of fluid refilling.

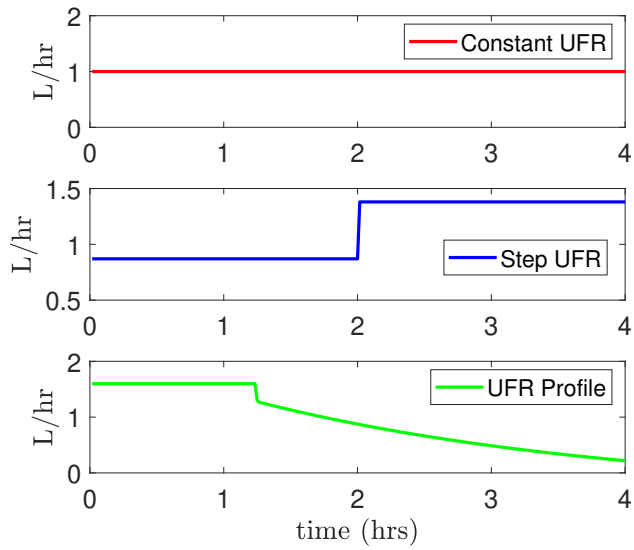

Figure 3. Top: A constant UFR profile, Middle: Step UFR profile, and Bottom: patient-specific (time-varying) profile used to explore the boundedness and behavior of the solution x during $0 \leq t < t_f$.

VI. Discussion

We presented global stability analysis for a specific class of nonlinear models used in dialysis treatment when the ultrafiltration is off. We were able to rearrange our model in this particular class of models and then apply these results to the model. We use qualitative properties of the net flow $G(x)$ and UFR profiles to ensure the boundedness of the solution of the model. The boundedness of the solution was derived based on physiological conditions applied in dialysis treatments. Our results indicate that if we start in the physiological set B_m, our model's solution trajectory never leaves this set.

For exploring the behavior of the solution under these UFR profiles, we compared the effect of these UFR profiles on the solution's trajectory $x(t)$ inside B_m during the dialysis therapy. The time-varying UFR profile, which was designed based on physiological insights from vascular refilling and bounds on fluid removal rates enables us to better understand fluid management during dialysis therapy.

VII. Conclusions

The current focus on improving fluid management in dialysis therapy motivated the need for exploring stability analysis for a specific class of models used in artificial kidney treatment in end-stage kidney disease patients.

This paper presented a novel global stability analysis for specific nonlinear multi-compartment models, which apply to our nonlinear two-compartment model. We demonstrated the boundedness of the solution under ultrafiltration profiles for the two-compartment model during dialysis therapy. We showed that under physiological conditions, the nonlinear model's solution can be bounded and contained in a pre-defined set during this therapy. We concluded that the nonlinear model's trajectories under the patient-specific UFR profile showed better behavior than the standard ultrafiltration

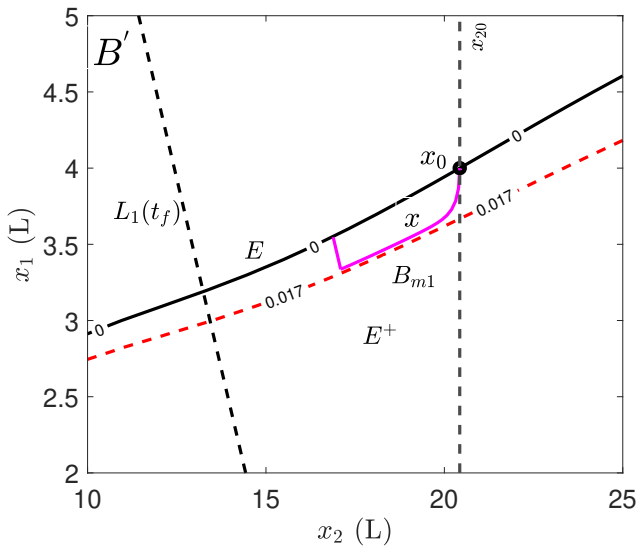

Figure 4. The solution $x(t)$ was contained in the set B_{m1} under the constant UFR profile. The set B_{m1} is determined as: $B_{m1} := \{x : 0 \leq G(x) \leq 0.017$ [L/min], $x_1 \leq 4$L, $x_2 \leq 20.4$L, and $L_1(t_f) = (x_1 + x_2) > 20.4L\}$, and $B^{'} \subset B$.

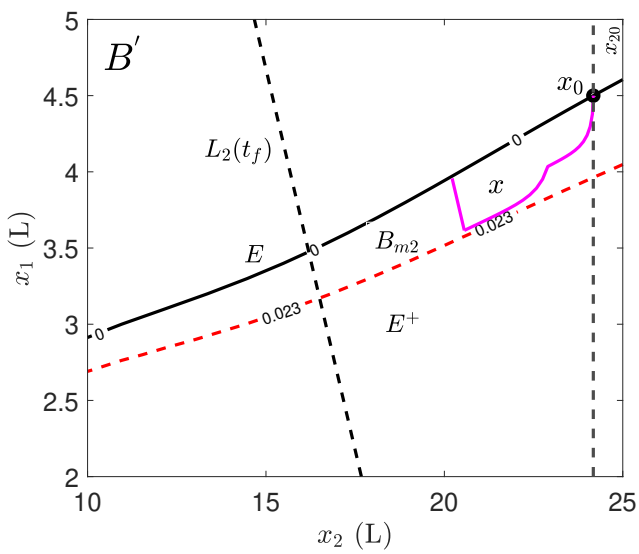

Figure 5. The solution $x(t)$ was contained in the set B_{m2} under the step UFR profile. The set $B_{m2} := \{x : 0 \leq G(x) \leq 0.023$[L/min], $x_1 \leq 4.5$L, $x_2 \leq 24.2$L, and $L_2(t_f) = (x_1 + x_2) > 24.2L\}$, and $B^{'} \subset B$.

profiles, and motivated us to provide new, more advanced therapeutics for hemodialysis, which could save numerous lives of people with end-stage kidney disease.

Appendix

A. Model Description:

From (2) we have

$$\delta_p(t) = (P_c(t) - P_i(t)) \tag{12a}$$

$$\delta_\pi(t) = (\pi_p(t) - \pi_i(t)) \tag{12b}$$

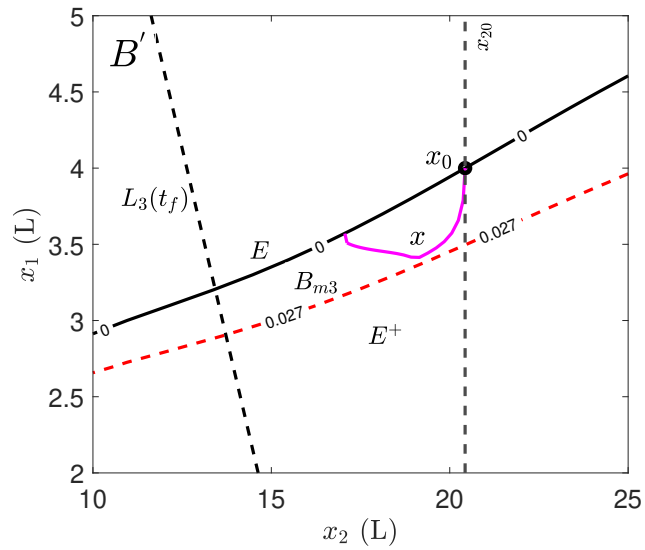

Figure 6. The solution x was contained in the set B_{m3} under the time-varying UFR profile. The B_{m3} is determined by $B_{m3} := \{x : 0 \leq G(x) \leq 0.027$[L/min], $x_1 \leq 4$L, $x_2 \leq 20.4$L, and $L_3(t_f) = (x_1 + x_2) > 20.6L\}$, and $B^{'} \subset B$.

where Pc, Pi, π_p, and π_i refer to the hydrostatic capillary pressure, interstitial pressure, plasma colloid osmotic pressure, and interstitial colloid osmotic pressure, respectively. The capillary pressure is defined by

$$P_c(t) = P_v(t) + P_{off}$$

$$P_v(t) = d\left(100\frac{V_{rbc} + x_1(t)}{V_{rbc} + V_{P,eu}} + r\right)^f \tag{13}$$

where P_v is the venous pressure, P_{off} is a pressure offset, $x_1(t)$ is the intravascular volume at a given time t, $V_{P,eu}$ is intravascular volume at the euhydrated state, d, e and l are constants [11] listed in Table I. We define

$$P_i(t) = a\Big((100\frac{x_2(t)}{V_{i,eu}}) + \frac{b}{(100\frac{ax_2(t)}{V_{i,eu}} + c)}\Big) \tag{14}$$

where $x_2(t)$ represents interstitial fluid volume at a given time t, $V_{i,eu}$ refers to interstitial volume at the euhydrated state, a, b and c are constants [11], and where

$$\pi_p(t) = \Big(\frac{k_{c1}m_p}{x_1(t)} + \frac{k_{c1}m_p^2}{x_1^2(t)} + \frac{k_{c1}m_p^3}{x_1^3(t)}\Big) \tag{15a}$$

$$\pi_i(t) = \Big(\frac{k_{c1}m_i}{x_2(t)} + \frac{k_{c1}m_i^2}{x_2^2(t)} + \frac{k_{c1}m_i^3}{x_2^3(t)}\Big) \tag{15b}$$

where m_p and m_i describe the protein mass in plasma and interstitial volumes, respectively, k_1, k_2 and k_3 are constants [20] (see Table I).

Since x_1 and x_2 represent volume, they should be positive. Hence, we will restrict the domain of x_1 and x_2 over this range $x_1 > 0$, $x_2 > 0$. Therefore, we set the term inside the bracket $(\cdot)$ in (13) to be greater than zero, then we solve for x_1 accordingly. We repeat this step for the denominator in (14) to solve for x_2. Note that the constants in (Table I) are used here. As a result, $Q_1(x)$ and $Q_2(x)$ are continuous in the following restricted domain:$x_1 \geq 1$ and $x_2 \geq 5$.

Table I
MODEL PARAMETERS

Parameter	Value	Parameter-Unit	Value
a	0.0065	K_f [L/min*mmHg]	0.0052
b	-146.3	$m_p[g]$	210
c	-54.72	$m_i[g]$	210
d	0.01	P_{off} [mmHg]	13
r	-30.0	k_1	0.21
f	1.5	k_2	0.0016
g	0.02	k_3	9e-6
h	0.63	$V_{P,eu}$ (L)	3
l	0.02	$V_{i,eu}$ (L)	12
-	-	V_{rbc} (L)	2

B. Compartmental Model Arrangement

We rearrange $Q_1(x)$ by separating the terms that contain x_1 and x_2 as follows: $Q_1(x_1, x_2) = K_f(P_c - \pi_p) - K_f(P_i - \pi_i)$ and then substitute the later $Q_1(x)$ in the model (3):

$$\begin{aligned}\dot{x}_1 =& - K_f\Big((P_c - \pi_p) - (P_i - \pi_i)\Big)\\ &+ (g\tanh(hP_i(t)) + l) - u\\ =& - \underbrace{K_f(P_c - \pi_p)}_{g_1(x_1)} +\\ &+ \underbrace{\Big(K_f(P_i - \pi_i) + g\tanh(hP_i(t)) + l\Big)}_{g_2(x_2)} - u\end{aligned}$$

and $\dot{x}_2$ becomes:

$$\begin{aligned}\dot{x}_2 =& K_f\Big((P_c - \pi_p) - K_f(P_i - \pi_i)\Big)\\ &- (g\tanh(hP_i(t)) + l) - u\\ =& \underbrace{K_f(P_c - \pi_p)}_{g_1(x_1)}\\ &- \underbrace{\Big(K_f(P_i - \pi_i) + g\tanh(hP_i(t)) + l\Big)}_{g_2(x_2)}\end{aligned}$$

that leads to

$$\dot{x}_1 = - g_1(x_1) + g_2(x_2) - u \tag{16a}$$
$$\dot{x}_2 = g_1(x_1) - g_2(x_2) \tag{16b}$$

where $g_1(x_1) = K_f(P_c - \pi_p)$ and $g_2(x_2) = K_f(P_i - \pi_i) + g\tanh(hP_i(t)) + l$.

C. Theorem 1

We have this Lyapunov candidate for n compartments:

$$V(x) = -\frac{1}{2} f(x)^T A_n f(x)$$

Substituting $f^T(x) = [\ f_1(x_1) \quad \dots \quad f_n(x_n)\ ]$ and A_n (4) into $V(x)$ leads to:

$$\begin{aligned}V(x) =& -\frac{1}{2}\Big(-a_{11}f_1^2(x_1) + \ldots + a_{1n}f_1(x_1)f_n(x_n)\\ &- a_{22}f_2^2(x_2) + \ldots + a_{2n}f_2(x_2)f_n(x_n)\\ &\vdots \qquad\qquad \vdots\\ &- a_{nn}f_n^2(x_n) + \ldots + a_{nn-1}f_n(x_n)f_{n-1}(x_{n-1})\Big)\end{aligned}$$

The derivative $\dot{V}(x)$ is:

$$\begin{aligned}\dot{V}(x) =& -\frac{1}{2}\Big(2\{-a_{11}f_1(x_1) + \ldots + a_{1n}f_n(x_n)\}\frac{\partial f_1(x_1)}{\partial x_1}\dot{x}_1\\ &+ 2\{-a_{22}f_2(x_2) + \ldots + a_{2n}f_n(x_n)\}\frac{\partial f_2(x_2)}{\partial x_2}\dot{x}_2\\ &\vdots \qquad\qquad \vdots\\ &+ 2\{-a_{nn}f_n(x_n) + a_{n1}f_1(x_1) + \ldots\\ &a_{nn-1}f_{n-1}(x_{n-1})\}\frac{\partial f_n(x_n)}{\partial x_n}\dot{x}_n\Big)\end{aligned}$$

This gives:

$$\begin{aligned}\dot{V}(x) =& -\Big(-a_{11}f_1(x_1) + \sum_{i\neq j}^{n} a_{1j}f_j(x_j)\frac{\partial f_1(x_1)}{\partial x_1}\dot{x}_1\\ &- a_{22}f_2(x_2) + \sum_{i\neq j}^{n} a_{2j}f_j(x_j)\frac{\partial f_2(x_2)}{\partial x_2}\dot{x}_2\\ &\vdots \qquad\qquad \vdots\\ &- a_{nn}f_n(x_n) + \sum_{i\neq j}^{n} a_{nj}f_j(x_j)\frac{\partial f_n(x_n)}{\partial x_n}\dot{x}_n\Big)\end{aligned}$$

From (3), we have the following:

$$\begin{aligned}-a_{11}f_1(x_1) + \sum_{i\neq j}^{n} a_{1j}f_j(x_j) &= \dot{x}_1\\ -a_{22}f_2(x_2) + \sum_{i\neq j}^{n} a_{2j}f_j(x_j) &= \dot{x}_2\\ \vdots \qquad\qquad &\vdots \quad \vdots\\ -a_{nn}f_n(x_n) + \sum_{i\neq j}^{n} a_{nj}f_j(x_j) &= \dot{x}_n\end{aligned}$$

Thus

$$\begin{aligned}\dot{V}(x) =& -\frac{\partial f_1(x_1)}{\partial x_1}\dot{x}_1 - \ldots - \frac{\partial f_n(x_n)}{\partial x_n}\dot{x}_n\\ =& -\sum_{i=1}^{n}\dot{x}_i\frac{\partial f_i(x_i)}{\partial x_i}\end{aligned}$$

D. Partial Derivative of the Flow

The partial derivative terms: $\frac{\partial g_i(x)}{\partial x_i}$, $i = 1, 2$ are derived here:

$$\begin{aligned}\frac{\partial g_1(x_1)}{\partial x_1} =& (\frac{K_f df 100}{(V_{rbc} + V_{p,eu})})\Big(100\frac{V_{rbc} + x_1(t)}{V_{rbc} + V_{p,eu}} + r\Big)^{f-1} +\\ &K_f\Big(\frac{k_{c1}m_p}{x_1(t)} + \frac{k_{c1}m_p^2}{x_1^2(t)} + \frac{k_{c1}m_p^3}{x_1^3(t)}\Big)\end{aligned} \tag{17}$$

and

$$\begin{aligned}\frac{\partial g(x_2)}{\partial x_2} =& \frac{K_f 100}{V_{i,eu}}\Big((100\frac{ax_2(t)}{V_{i,eu}}) - \frac{b}{(100\frac{ax_2(t)}{V_{i,eu}}+c)^2}\Big)\\ &+ K_f\Big(\frac{k_{c1}m_i}{x_2(t)} + \frac{k_{c1}m_i^2}{x_2^2(t)} + \frac{k_{c1}m_i^3}{x_2^3(t)}\Big)\\ &+ g\text{sech}^2\Big(ha(100\frac{ax_2(t)}{V_{i,eu}}) + \frac{b}{(100\frac{ax_2(t)}{V_{i,eu}}+c)}\Big)\\ &\Big(\frac{K_f 100}{V_{i,eu}}\Big((100\frac{ax_2(t)}{V_{i,eu}}) - \frac{b}{(100\frac{ax_2(t)}{V_{i,eu}}+c)^2}\Big)\Big)\end{aligned} \tag{18}$$

Using the parameters in Table I, we have: $\frac{\partial f_1(x_1)}{\partial x_1} > 0$ and $\frac{\partial f_2(x_2)}{\partial x_2} > 0$. Note that since $G(x) = -g_1(x_1) + g_2(x_2)$, then $G_{x_1} = \frac{\partial G(x)}{\partial x_1} < 0$ and $G_{x_2} = \frac{\partial G(x)}{\partial x_1} > 0$.

E. Theorem2 (proof)

Substituting $G(x) = -g_1(x_1) + g_2(x_2)$ into (5) leads to

$$\begin{aligned}\dot{x_1} &= G(x) - u\\ \dot{x_2} &= -G(x)\end{aligned} \tag{19}$$

and then

$$E := \{x : G(x) = 0\}.$$

Proof: Along the solution to (5), $\dot{Q}$ is given by

$$\begin{aligned}\dot{G} &= (G_{x_1}\dot{x}_1 + G_{x_2}\dot{x}_2)\\ &= (G_{x_1}(G-u) + G_{x_2}(-G))\\ &= (G_{x_1} - G_{x_2})G - G_{x_1}u(t)\end{aligned} \tag{20}$$

a) At $G(x) = 0$, from (20) and condition (1), $\dot{G} = -G_{x_1}u(t)$:

$$\dot{G} = \begin{cases} -G_{x_1}u_{max} > 0, & 0 < t \le t^*\\ -G_{x_1}\hat{u}(t) \ge 0 & t^* < t \le t_f.\end{cases} \tag{21}$$

b) Using $G(x) = u_{max}$, from (20) and condition (2) $\dot{G} = G_{x_1}(u_{max} - u(t)) - G_{x_2}u_{max}$:

$$\dot{G} = \begin{cases} -G_{x_2}u_{max} < 0, & 0 < t \le t^*\\ (G_{x_1}(u_{max} - \hat{u}(t)) - G_{x_2 u_{max}}) < 0 & t^* < t \le t_f.\end{cases} \tag{22}$$

c) Using $G(x) \le u_{max}$, it follows:

$$\begin{aligned}G(x) - u(t) &\le u_{max} - u(t)\\ \dot{x}_1 &\le u_{max} - u(t)\\ x_1 &\le x_{10} - \int_{\hat{u}(t^*)}^{\hat{u}(t)} \hat{u}(s)ds\\ &\le x_{10}\end{aligned} \tag{23}$$

d) and using $G(x) \ge 0$, it follows:

$$\begin{aligned}-G(x) &\le 0\\ \dot{x}_2 &\le 0\\ x_2(t) &\le x_{20}\end{aligned} \tag{24}$$

From (5), we have

$$\dot{x}_1 + \dot{x}_2 = -u(t)$$

then

$$\begin{aligned}x_1 + x_2 &= (x_{10} + x_{20}) - (u_{max}t + \int_{\hat{u}(t^*)}^{\hat{u}(t)} \hat{u}(s)ds)\\ &> (x_{10} + x_{20}) - (u_{max}t^* + \int_{\hat{u}(t^*)}^{\hat{u}(t)} \hat{u}(s)ds)\end{aligned}$$

then from a, b, and d: $x(t) \in B_m$, for all $0 \le t \le t_f$. This proves the Theorem. ■

References

[1] Rammah Abohtyra, Yossi Chait, Michael J Germain, Christopher V Hollot, and Joseph Horowitz. Individualization of ultrafiltration in hemodialysis. *IEEE Transactions on Biomedical Engineering*, 66(8):2174–2181, 2018.

[2] Rammah Abohtyra, CV Hollot, Michael G Germain, Yossi Chait, and Joseph Horowitz. Personalized ultrafiltration profiles to minimize intradialytic hypotension in end-stage renal disease. In *2018 IEEE Conference on Decision and Control (CDC)*, pages 309–314. IEEE, 2018.

[3] John WM Agar. Personal viewpoint: Limiting maximum ultrafiltration rate as a potential new measure of dialysis adequacy. *Hemodialysis International*, 20(1):15–21, 2016.

[4] A Aurelio, Doris H Fuertinger, Franz Kappel, Anna Meyring-Wösten, Stephan Thijssen, and Peter Kotanko. A physiologically based model of vascular refilling during ultrafiltration in hemodialysis. *Journal of theoretical biology*, 390:146–155, 2016.

[5] Reginald F Brown. Compartmental system analysis: State of the art. *IEEE Transactions on Biomedical Engineering*, (1):1–11, 1980.

[6] PW Chamney, C Johner, C Aldridge, M Kramer, N Valasco, JE Tattersall, T Aukaidey, R Gordon, and RN Greenwood. Fluid balance modelling in patients with kidney failure. *Journal of medical engineering & technology*, 23(2):45–52, 1999.

[7] Airlie Chapman and Mehran Mesbahi. Stability analysis of nonlinear networks via m-matrix theory: Beyond linear consensus. In *2012 American Control Conference (ACC)*, pages 6626–6631. IEEE, 2012.

[8] Sarah Faubel and Joel Topf. *The fluid, electrolyte & acid-base companion*. Alert and Oriented Pub., 1999.

[9] Jurgen Floege, Richard J Johnson, and John Feehally. *Comprehensive clinical nephrology*. Elsevier Health Sciences, 2010.

[10] Jennifer E Flythe, Matthew J Tugman, Julia H Narendra, Magdalene M Assimon, Quefeng Li, Yueting Wang, Steven M Brunelli, and Alan L Hinderliter. Effect of ultrafiltration profiling on outcomes among maintenance hemodialysis patients: a pilot randomized crossover trial. *Journal of Nephrology*, pages 1–11, 2020.

[11] Aimee Stasia Goncalves. Model-based feedback control for hemodialysis treatment of chronic kidney disease patients, 2015.

[12] AC Guyton and JE Hall. Textbook of medical physiology (9th edn) wb saunders company. *Philadelphia. Pennsylvania*, page 1006, 1996.

[13] Arthur C Guyton and JE Hall. The body fluid compartments: extracellular and intracellular fluids; interstitial fluid and edema. *Textbook of medical physiology*, 11:293, 2000.

[14] Wassim M Haddad, Tomohisa Hayakawa, and James M Bailey. Adaptive control for non-negative and compartmental dynamical systems with applications to general anesthesia. *International journal of adaptive control and signal processing*, 17(3):209–235, 2003.

[15] John E Hall. *Pocket companion to Guyton & Hall textbook of medical physiology*. Elsevier Health Sciences, 2015.

[16] John A Jacquez and Carl P Simon. Qualitative theory of compartmental systems. *Siam Review*, 35(1):43–79, 1993.

[17] Jack Q Jaeger and Ravindra L Mehta. Assessment of dry weight in hemodialysis: an overview. *Journal of the American Society of Nephrology*, 10(2):392–403, 1999.

[18] PR Keshaviah, KM Ilstrup, and FL Shapiro. Dynamics of vascular refilling. *Artif. Organs*, 2:506–10, 1983.

[19] Hassan K Khalil and JW Grizzle. *Nonlinear systems*, volume 3. Prentice hall New Jersey, 1996.

[20] EM Landis and JR Pappenheimer. Exchange of substances through the capillary walls. *Handbook of physiology*, 2(2):961–1034, 1963.

[21] Jing Lin, Zhen Cheng, Xiaoqiang Ding, and Qi Qian. Acid-base and electrolyte managements in chronic kidney disease and end-stage renal disease: Case-based discussion. *Blood purification*, 45(1-3):179–186, 2018.

[22] Hajime Maeda and Shinzo Kodama. Qualitative analysis of a class of nonlinear compartmental systems: nonoscillation and asymptotic stability. *Mathematical Biosciences*, 38(1):35–44, 1978.

[23] Hajime Maeda, Shinzo Kodama, and Yuzo Ohta. Asymptotic behavior of nonlinear compartmental systems: nonoscillation and stability. *Circuits and Systems, IEEE Transactions on*, 25(6):372–378, 1978.

[24] Stefano Marano, Marco Marano, and Leandro Pecchia. Frontiers in hemodialysis part ii: Toward personalized and optimized therapy. *Biomedical Signal Processing and Control*, 61:102029, 2020.

[25] Susumu Ookawara, Kiyonori Ito, Takayuki Uchida, Keito Tokuyama, Satoshi Kiryu, Takeshi Suganuma, Kyoko Hojyo, Haruhisa Miyazawa, Yuichiro Ueda, Chiharu Ito, et al. Hemodialysis crossover study using a relative blood volume change-guided ultrafiltration control compared with standard hemodialysis: the bv-ufc study. *Renal Replacement Therapy*, 6(1):1–10, 2020.

[26] Biff F Palmer and William L Henrich. Recent advances in the prevention and management of intradialytic hypotension. *Journal of the American Society of Nephrology*, 19(1):8–11, 2008.

[27] Donal N Reddan, Lynda Anne Szczech, Vic Hasselblad, Edmund G Lowrie, Robert M Lindsay, Jonathan Himmelfarb, Robert D Toto, John Stivelman, James F Winchester, Linda A Zillman, et al. Intradialytic blood volume monitoring in ambulatory hemodialysis patients: a randomized trial. *Journal of the American Society of Nephrology*, 16(7):2162–2169, 2005.

[28] Patrick B Reeves and Finnian R Mc Causland. Mechanisms, clinical implications, and treatment of intradialytic hypotension. *Clinical journal of the American Society of Nephrology*, 13(8):1297–1303, 2018.

[29] John A Sargent, Marco Marano, Stefano Marano, and F John Gennari. Acid-base homeostasis during hemodialysis: New insights into the mystery of bicarbonate disappearance during treatment. In *Seminars in dialysis*, volume 31, pages 468–478. Wiley Online Library, 2018.

[30] Daniel Schneditz, Johannes Roob, Martina Oswald, Helmuth Pogglitsch, Maximilian Moser, Thomas Kenner, and Ulrich Binswanger. Nature and rate of vascular refilling during hemodialysis and ultrafiltration. *Kidney international*, 42(6):1425–1433, 1992.

[31] Kaoru Tabei, Hirofumi Nagashima, Osamu Imura, Toshihiro Sakurai, and Yasushi Asano. An index of plasma refilling in hemodialysis patients. *Nephron*, 74(2):266–274, 1996.

[32] Mathukumalli Vidyasagar. *Nonlinear systems analysis*, volume 42. Siam, 2002.